Electrical Power and Energy Systems 172 (2025) 111144

Contents lists available at ScienceDirect

International Journal of Electrical Power and Energy Systems

journal homepage: www.elsevier.com/locate/ijepes

Risk of oscillations induced collectively by multiple DFIGs and PMSGs in a wind power collecting system

Zhengnan Zhao [a], Wenjuan Du [a,*], Qiang Fu [b], Xiao Chen [c], Yijun Wang [d], H.F. Wang [a]

[a] School of Electrical Engineering, Sichuan University, Chengdu, 610065, Sichuan Province, China
[b] School of Department of Electrical and Electronic Engineering, Hong Kong Polytechnic University, Kowloon, 999077, Hong Kong, China
[c] North China Branch of State Grid Corporation of China, Beijing, 100051, China
[d] China Electric Power Planning & Engineering Institute, Beijing, 100031, China

ARTICLE INFO

Keywords:
WTGs
Dynamics interaction
Wind power collecting system
Collective oscillation risk

ABSTRACT

It has been found that same type of multiple wind turbine generators (WTGs), either PMSGs or DFIGs, in a grid-connected wind farm may collectively cause growing oscillations. This paper investigates the risk of oscillations induced collectively by both the DFIGs and PMSGs in a wind power collecting system (WPCS). Analysis is carried out to indicate that if the PMSGs and the DFIGs happen to have components, such as the phase-locked loops (PLLs) or converter control loops, bandwidths of which fall in the same range such that their dynamics are similar, it is possible that multiple DFIGs and PMSGs may jointly induce growing oscillations. Three study cases are presented to validate and demonstrate the analysis and conclusions made in the paper about dynamics interactions between (1) The PLLs equipped by multiple DFIGs and PMSGs; (2) The PLLs of a group of the DFIGs and the DC voltage control loops of another cluster of the PMSGs. The DFIGs and the PMSGs collectively cause growing oscillations, though the dynamics of the DFIGs and PMSGs are completely different. The oscillation risk increases when more DFIGs or/and PMSGs are connected in the WPCS.

1. Introduction

1.1. Literature review

As large-scale wind power continues to integrate into the grid, the risk of oscillatory instability it brings about increases [1–4]. To examine the potential for oscillatory instability induced by grid-connected wind turbine generators (WTG), the impedance model-based method (IMA) has been widely adopted [5–8]. The IMA usually decomposes a power system containing grid-connected WTGs into a source impedance and a load impedance. Afterwards, the generalized Nyquist criterion is applied to the interconnected model of the source and the load impedance model to determine the system stability [9–12]. To understand the mechanism behind why a WTG may cause oscillatory instability, the two-input two-output interconnected model of the source and load impedance has to be simplified under certain assumptions to a single-input single-output (SISO) interconnected model. Subsequently, analysis can conclude that if the WTG exhibits as negative resistance, the oscillatory instability occurs. This general analysis of oscillatory instability mechanism by use of the IMA has been successfully applied to a single grid-connected WTG system with many useful conclusions obtained [13–17].

The open-loop mode analysis (OMA) employs modal analysis techniques to evaluate the risk of oscillatory instability. It divides the grid-connected power system with WTGs into two interconnected subsystems and attributes the oscillatory instability to resonance in the open-loop model. It can reveal the mechanism of oscillatory instability caused by two grid-connected WTGs from the perspective of modal resonance. That is an open-loop oscillation mode of one WTG is near to an open-loop oscillation mode of another WTG on the complex plane [18–23]. Hence, the OMA explains why dynamic interactions between two WTGs may bring about the oscillatory instability in the power system.

In [24–26], the oscillatory instability of a grid-connected wind farm with the same type of WTGs, either PMSGs or DFIGs, is examined. The examination reveals that if the WTGs are of similar dynamics, they collectively may cause oscillatory instability and the risk of oscillatory instability increases when more WTGs of the same type, either PMSGs or DFIGs with similar dynamics, are connected in the wind farm. The phenomenon of this collective impact was reported in [24] initially. In [25,26], general analysis is carried out to reveal that the small-signal stability of a grid-connected wind farm is constrained by not only the load level and the converter control system settings of the

* Corresponding author.
E-mail address: ddwenjuan@qq.com (W. Du).

https://doi.org/10.1016/j.ijepes.2025.111144
Received 30 March 2025; Received in revised form 15 August 2025; Accepted 11 September 2025
Available online 24 September 2025

WTGs, as well as the status of the wind farm's grid connection, but also by the number of WTGs of the same type with similar dynamics. The analytical conclusions obtained in [24–26] are meaningful, as in practice the WTGs in a wind farm may be of the same type supplied by a same manufacturer. The dynamics of the WTGs may be possibly similar. Hence, special attention should be paid to the risk of oscillatory instability collectively caused by multiple the same type of the WTGs with similar dynamic, both during the planning phase and in the operational stage of grid-connected wind farm.

1.2. Contributions and the organization of the paper

In a grid-connected wind power collecting system (WPCS) comprising multiple wind farms, the WTGs usually are of different types, either PMSGs or DFIGs. As being reviewed above, studies so far have indicated that if a grid-connected WTG exhibits as negative resistance, or open-loop modal resonance between two grid-connected WTGs happens, or the WTGs in a grid-connected wind farm are of the same type and similar dynamics, those WTGs are possibly the trouble makers to induce growing oscillations in the WPCS. We may wonder if there are any other possibility that the WTGs in the WPCS may introduce the risk of oscillations and that we need to pay special attention to? If the answer is yes, then why? This paper attempts to investigate the answers to the questions and reports the following important finding of the investigation:

In the WPCS, it is possible that bandwidths of certain dynamic components of the DFIGs and those of the PMSGs may happen to fall in the same range, thought the DFIGs and the PMSGs are different type of the WTGs and their dynamics as a whole are completely different. For example, the bandwidths of the PLLs of a group of the DFIGs and the PLLs of a cluster of the PMSGs may be of the similar bandwidths. This is because the requirements of the speed and accuracy of voltage phase tracking for the PLLs of the DFIGs and the PMSGs are similar. Subsequently, dynamics of the components with similar bandwidth are similar. Analysis carried out in the paper indicates and elaborates that in this case, different types of the WTGs, i.e., the DFIGs and PMSGs, may collectively induce growing oscillations in the WPCS. The trouble makers are the components with similar dynamics of the DFIGs and the PMSGs. Risk of oscillations increases when more such different type of the WTGs are connected.

Main contributions of the paper are as follows:

Conclusions obtained in [24–26] about the collective impact of the same types of the WTGs with similar dynamics in a wind farm connected to the grid, either the PMSGs and the DFIGs, are extended to the case of different types of the WTGs, both the PMSGs and the DFIGs, in the WPCS comprising multiple grid-connected wind farms. The extension calls upon special attentions paid on the risk of oscillatory instability associated with the collective impact of different types of the WTGs. In the practical operation, if it is found that when more WTGs, both the PMSGs and the DFIGs, are connected, growing oscillations occur, it is highly possible that the growing oscillations are caused by the collective impact of both the PMSGs and the DFIGs, as being reported and analyzed in the paper. Subsequently, further in-depth examination is needed to check if those PMSGs and DFIGs are of the components with similar dynamics. Afterwards, necessary parameters adjustment of the components is needed to dismiss the risky collective impact. At the stage of planning the WPCS, guidance is provided to avoid the PMSGs and the DFIGs to be of the components with similar dynamics. Otherwise, the scale of the WPCS will be constrained by the risk of oscillatory instability caused by the collective impact of the PMSGs and the DFIGs.

Organization of the paper is as follows. In the next section, firstly mathematical model of the WPCS with both the PMSGs and the DFIGs is established. Secondly, analysis is carried out to indicate that if the PMSGs and the DFIGs are of the components with identical dynamics, it is possible that the PMSGs and the DFIGs may collectively induce growing oscillations in the WPCS. Thirdly, analysis is extended to the case that the dynamics of the components are similar instead of identical to explain why the collective impact of the PMSGs and the DFIGs may be dangerous. For the simplicity of mathematically presenting the analysis, the PLLs are used as the representatives of the components causing the collective impact. Another case of the collective impact of the DC voltage control loops of the PMSGs and the PLLs of the DFIGs, which happen to have the same bandwidth, is also analyzed. In Section 3 of the paper, three study cases are presented to validate and demonstrate the analysis and conclusions made. Final section of the paper summarizes the main conclusions made in the paper. Practical significance of the study carried out in the paper to guide the operation and planning of the WPCS is discussed.

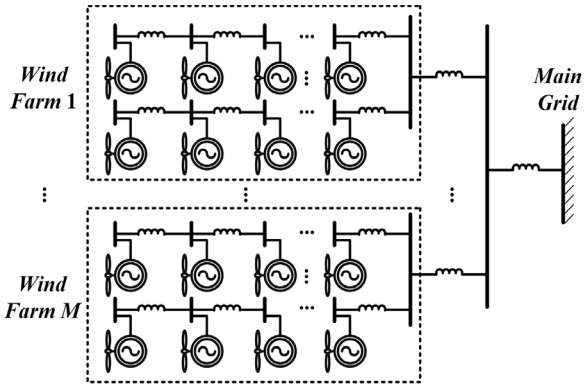

Fig. 1. Configuration of a WPCS.

2. Collective impact of the PMSGs and the DFIGs

2.1. Full-order model of a WPCS with the PMSGs and the DFIGs

Fig. 1 illustrates the configuration of a WPCS, consisting of M wind farms. The total number of the WTGs is N. The state–space model for the kth WTG is [27]:

$$\begin{cases} \frac{d}{dt}\Delta \boldsymbol{X}_k = \boldsymbol{A}_k \Delta \boldsymbol{X}_k + \boldsymbol{B}_k \Delta \boldsymbol{V}_k \\ \Delta \boldsymbol{I}_k = \boldsymbol{C}_k \Delta \boldsymbol{X}_k + \boldsymbol{D}_k \Delta \boldsymbol{V}_k \end{cases}, k = 1, 2, \ldots, N \tag{1}$$

where $\Delta \boldsymbol{X}_k$ represents the state variable vector of the k th WTG. $\Delta \boldsymbol{I}_k = [\Delta I_{xk} \quad \Delta I_{yk}]^T$ and $\Delta \boldsymbol{V}_k = [\Delta V_{xk} \quad \Delta V_{yk}]^T$, $V_{xk} + jV_{yk}$ and $I_{xk} + jI_{yk}$ represent respectively the terminal voltage and output current of the kth WTG in the standard x-y coordinate system. The network voltage equations can be expressed after linearization as:

$$\Delta \boldsymbol{I} = \boldsymbol{Y}_{net} \Delta \boldsymbol{V} \tag{2}$$

where $\Delta \boldsymbol{I} = [\Delta \boldsymbol{I}_1^T \quad \Delta \boldsymbol{I}_2^T \cdots \Delta \boldsymbol{I}_N^T]^T$, $\boldsymbol{Y}_{net}$ represents the network admittance matrix, $\Delta \boldsymbol{V} = [\Delta \boldsymbol{V}_1^T \quad \Delta \boldsymbol{V}_2^T \cdots \Delta \boldsymbol{V}_N^T]^T$.

The model of the WPCS can be derived from Eqs. (1) and (2) to be [28,29]:

$$\frac{d}{dt}\Delta \boldsymbol{X} = \boldsymbol{A} \Delta \boldsymbol{X} \tag{3}$$

where $\Delta \boldsymbol{X} = [\Delta \boldsymbol{X}_1^T \quad \Delta \boldsymbol{X}_2^T \cdots \Delta \boldsymbol{X}_M^T]^T$, $\boldsymbol{A} = diag[\boldsymbol{A}_k] + diag[\boldsymbol{B}_k](\boldsymbol{I} - \boldsymbol{Y}_{net}^{-1} diag[\boldsymbol{D}_k])^{-1} diag[\boldsymbol{C}_k]$, where $diag[\bullet]$ represents a block diagonal matrix.

In the following first two subsections, analysis is carried out to indicate that both the PMSGs and the DFIGs in the WPCS may collectively induce growing oscillations if any components of the PMSGs and the DFIGs are of the similar dynamics. In order to clearly present the mathematical derivations in the analysis, the PLLs are selected as a kind of representatives of the components. Hence, in the following Section 2.2, a theoretical case of the PLLs with identical dynamics is

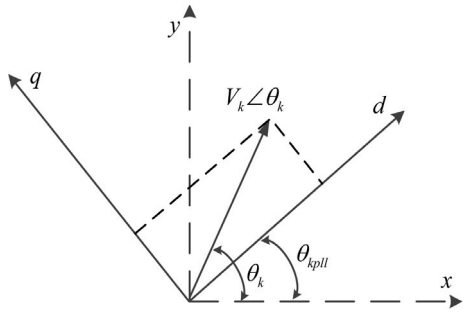

Fig. 2. Principle of the PLL for voltage phase tracking.

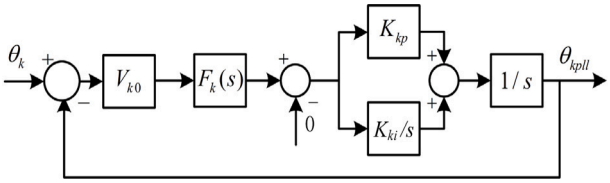

Fig. 3. Control structure diagram of the SRF-PLL.

examined firstly in order to simplify the presentation of the derivations. Whilst in Section 2.3, the practical case of the PLLs with similar dynamics is studied.

The analysis conducted in Section 2.3 is similarly applicable if the components are the different types of parts of the PMSGs and the DFIGs instead of the PLLs. Hence, Section 2.4 presents the case that the DC voltage control outer loops of the PMSGs and the PLLs equipped by the DFIGs in a WPCS are the components of the PMSGs and the DFIGs with the similar dynamics, which may induce growing oscillations due to their collective impact.

2.2. Risk of oscillatory instability brought about collectively by the PMSGs and the DFIGs — their PLLs are of identical dynamics

A PLL tracks the grid-point voltage phase of a WTG to ensure that the grid-point voltage and the d-axis position of the WTG coincide, thereby enabling the decoupled control of active and reactive power, as depicted in Fig. 2. Here, $V_k\angle\theta_k$ represents the grid-point voltage of the kth WTG, θ_k is the phase of the grid-point voltage of the kth WTG in the x-y coordinate system, and θ_{kpll} is the phase of the grid-point voltage tracked by the PLL.

There are various types of PLLs. In this paper, the most common type of the PLL, the synchronous reference frame PLL (SRF-PLL), is used. The structure of the SRF-PLL is illustrated in Fig. 3 [30]. The dynamic relationship between the input θ_k and the output θ_{kpll} of the kth PLL is given by the following equation:

$$\Delta\theta_{kpll} = P_k(s)\Delta\theta_k \tag{4}$$

where $P_k(s)$ represents the PLL's transfer function.

$P_k(s)$ can be expressed as:

$$P_k(s) = \frac{V_{k0}F_k(s)(K_{kp}s + K_{ki})}{s^2 + V_{k0}F_k(s)K_{kp}s + V_{k0}F_k(s)K_{ki}} \tag{5}$$

where K_{kp} and K_{ki} are PI gains of the kth PLL respectively, V_k is the magnitude of grid-point voltage of the kth WTG, 0 denotes the steady-state value of a variable, $F_k(s)$ represents a low-pass filter.

When there are L dynamically similar PLLs equipped by the PMSGs and/or the DFIGs within the WPCS:

$$P_1(s) \approx P_2(s) \approx \cdots P_L(s), L \le N \tag{6}$$

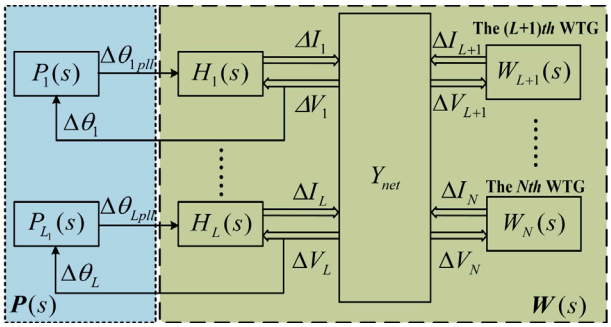

Fig. 4. Division of the WPCS with L similar PLLs.

We can divide the WPCS into two subsystems: one composed of similar PLLs denoted as subsystem $\boldsymbol{P}(s)$, and the other consisted of the remaining system referred to as subsystem $\boldsymbol{W}(s)$. Here, $\boldsymbol{P}(s) = diag[P_k(s)], k = 1, 2, \ldots, L$. Consequently, for these two subsystems, we have:

$$\Delta\boldsymbol{\theta} = \boldsymbol{W}(s)\Delta\boldsymbol{\theta}_p \tag{7}$$

$$\Delta\boldsymbol{\theta}_p = \boldsymbol{P}(s)\Delta\boldsymbol{\theta} \tag{8}$$

where $\Delta\boldsymbol{\theta}_p = [\Delta\theta_{1pll} \quad \Delta\theta_{2pll} \cdots \Delta\theta_{Lpll}]^T$, $\Delta\boldsymbol{\theta} = [\Delta\theta_1 \quad \Delta\theta_2 \cdots \Delta\theta_L]^T$.

Fig. 4 illustrates the division of L similar PLLs and the remaining system. Here, $H_k(s), k = 1, 2 \cdots L$ represents the transfer function of the remaining part of the kth WTG, excluding the PLL. Y_{net} denotes the network admittance matrix of the WPCS after linearization, and $W_l(s), l = L+1, L+2 \cdots N$ denotes the transfer function of the remaining WTGs in the system.

Let $\lambda_i = \xi_i + j\omega_i$ be an oscillation mode of the WPCS, then:

$$Det\{\boldsymbol{I} - diag[P_k(\lambda_i)]\boldsymbol{W}(\lambda_i)\} = 0 \tag{9}$$

where $\boldsymbol{I}$ is a unit matrix; $Det\{\bullet\}$ refers to the determinant of a matrix.

Let $\eta_j, j = 1, 2, \ldots, L$ be the eigenvalues of $\boldsymbol{W}(\lambda_i)$. Hence, there exists a matrix $\boldsymbol{T}$ that satisfies the following relationship:

$$\boldsymbol{T}\boldsymbol{W}(\lambda_i)\boldsymbol{T}^{-1} = diag[\eta_j] \tag{10}$$

Consider a theoretical case that L PLLs are dynamically identical, satisfying:

$$P_1(s) = P_2(s) = \cdots P_L(s), L \le N \tag{11}$$

Using the Lth PLL as the averaged model to represent all the other PLLs, we have:

$$\Delta\boldsymbol{\theta}_p = diag[P_L(s)]\Delta\boldsymbol{\theta} \tag{12}$$

In the PLL, a low-pass filter is commonly employed to eliminate high-frequency harmonics exceeding 300 Hz. We can assume $F_k(s) = 1$, then from Fig. 3 we have:

$$P_L(s) = \frac{V_{L0}(K_{Lp}s + K_{Li})}{s^2 + V_{L0}K_{Lp}s + V_0K_{Li}} \tag{13}$$

Multiplying both sides of (9) on the left by $\boldsymbol{T}$ and on the right by $\boldsymbol{T}^{-1}$, we have:

$$Det\{\boldsymbol{I} - diag[P_L(\lambda_i)]diag[\eta_j]\} = 0 \tag{14}$$

Then, there exists a n_j that satisfies the following equation:

$$1 - P_L(\lambda_i)\eta_j = 0, j = 1, 2, \ldots, N \tag{15}$$

Combining Eqs. (13) and (15), we have:

$$\lambda_i^2 - (\eta_j - 1)V_{L0}K_{Lp}\lambda_i - (\eta_j - 1)V_{L0}K_{Li} = 0 \tag{16}$$

Therefore, we can obtain:

$$\lambda_i = \frac{1}{2}[V_{L0}K_{Lp}(\eta_j - 1) \pm j\sqrt{V_{L0}{}^2K_{Lp}{}^2(\eta_j - 1)^2 + 4V_{L0}K_{Li}(\eta_j - 1)}] \tag{17}$$

From Eq. (17), it is evident that the risk of oscillatory instability introduced by L identical dynamic PLLs is influenced by two key factors. The first factor is the PI gain of the PLL, and the second factor is the dynamic interaction between L PLLs and the rest of the WPCS, denoted as n_j. Under the combined influence of these two factors, situations may arise that the oscillation mode, $\lambda_i = \xi_i + j\omega_i$, is located in the right-had half of the complex plane, causing multiple L PLLs with identical dynamics to collectively induce oscillatory instability.

2.3. Risk of oscillatory instability brought about collectively by the PMSGs and the DFIGs — their PLLs are of similar dynamics

When dynamics of L PLLs are similar rather than identical, we use the transfer function $P_n(s)$ of the nth PLL as the average model, replacing $P_L(s)$ in the derivations in the previous subsection. Then, for the remaining PLLs with similar dynamics, we have:

$$\Delta P_k(s) = P_n(s) - P_k(s); k = 1, 2, \dots, L \tag{18}$$

where $\Delta P_k(s), k = 1, 2, \dots, L$ represents the deviation between the kth PLL and the averaged model $P_n(s)$ used. Therefore, for the kth PLL, the output deviation $\Delta\theta_{ke}$ can be expressed as:

$$\Delta\theta_{ke} = \Delta\theta_{knpll} - \Delta\theta_{kpll} \tag{19}$$

where $\Delta\theta_{knpll}$ represents the grid-point voltage phase tracked by the kth PLL when using the averaged model, and for the kth PLL:

$$\Delta\theta_{knpll} = P_n(s)\Delta\theta_k \tag{20}$$

So, by combining Eq. (4) with Eq. (20), we can obtain:

$$\Delta\theta_{ke} = \Delta P_k(s)\Delta\theta_k \tag{21}$$

Therefore, we have:

$$\Delta\boldsymbol{\theta}_e = diag[\Delta P_k(s)]\Delta\boldsymbol{\theta} \tag{22}$$

where $\Delta\boldsymbol{\theta}_e = [\Delta\theta_{1e} \quad \Delta\theta_{2e} \cdots \Delta\theta_{Le}]^T$. Subsequently,we can obtain::

$$\Delta\boldsymbol{\theta} = \boldsymbol{W}(s)(\Delta\boldsymbol{\theta}_{np} - \Delta\boldsymbol{\theta}_p) \quad = \boldsymbol{W}(s)\Delta\boldsymbol{\theta}_{np} - \boldsymbol{W}(s)diag[\Delta P_k(s)]\Delta\boldsymbol{\theta} \tag{23}$$

where $\Delta\boldsymbol{\theta}_{np} = \left[\Delta\theta_{1npll} \quad \Delta\theta_{2npll} \cdots \Delta\theta_{Lnpll}\right]^T$. Hence, we have:

$$\Delta\boldsymbol{\theta} = \{\boldsymbol{I} + \boldsymbol{W}(s)diag[\Delta P_k(s)]\}^{-1}\boldsymbol{W}(s)\Delta\boldsymbol{\theta}_{np} \tag{24}$$

For an oscillation mode of the WPCS, $\tilde{\lambda}_i = \tilde{\xi}_i + j\tilde{\omega}_i$, by using Eqs. (22) and (24), we have:

$$Det\left\{\boldsymbol{I} - diag[P_n(\tilde{\lambda}_i)]\boldsymbol{W}(\tilde{\lambda}_i)\right\} = 0 \tag{25}$$

where $\tilde{\boldsymbol{W}}(\tilde{\lambda}_i) = \{\boldsymbol{I} + \boldsymbol{W}(\tilde{\lambda}_i)diag[\Delta P_k(\tilde{\lambda}_i)]\}^{-1}\boldsymbol{W}(\tilde{\lambda}_i)$.

Let $\tilde{\eta}_j, j = 1, 2, \dots, L$ be the eigenvalues of $\tilde{\boldsymbol{W}}(\tilde{\lambda}_i)$. Similar to the derivation from (10) to (17), we can obtain:

$$\tilde{\lambda}_i = \frac{1}{2}[V_{n0}K_{np}(\tilde{\eta}_j - 1) \pm j\sqrt{V_{n0}^2K_{np}^2\left(\tilde{\eta}_j - 1\right)^2 + 4V_{n0}k_{ni}\left(\tilde{\eta}_j - 1\right)}] \tag{26}$$

Obviously, it can be seen that in the worst case, L dynamically similar PLLs may induce oscillations in the WPCS when $\tilde{\lambda}_i = \tilde{\xi}_i + j\tilde{\omega}_i$ is in the right-hand half of complex plane.

2.4. Risk of oscillatory instability brought about collectively by the PMSGs and the DFIGs — the DC voltage control outer loops of the PMSGs and the PLLs equipped by the DFIGs are of similar dynamics

Fig. 5 illustrates the configuration of the grid side converter (GSC) for the kth PMSG in the WPCS. The linearized DC voltage equation can be described by the following equation:

$$\Delta V_{kdc} = \frac{1}{CV_{kdc0}s}(\Delta P_{kr} - \Delta P_{kg}) \tag{27}$$

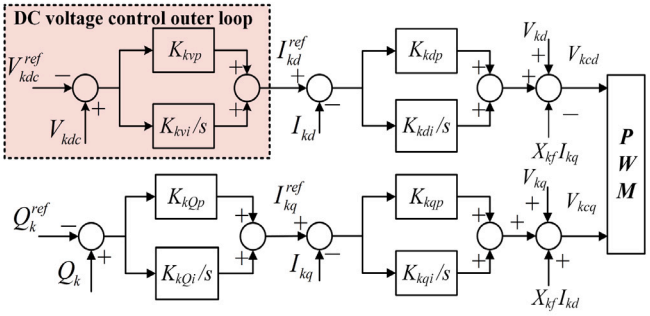

Fig. 5. Configuration of the GSC.

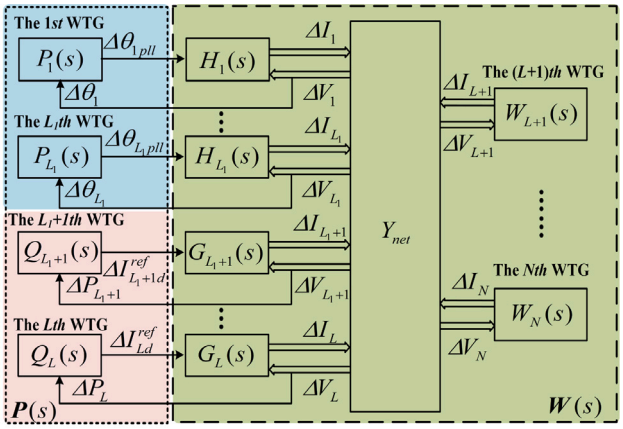

Fig. 6. Division of the WPCS with L components of similar dynamic characteristics.

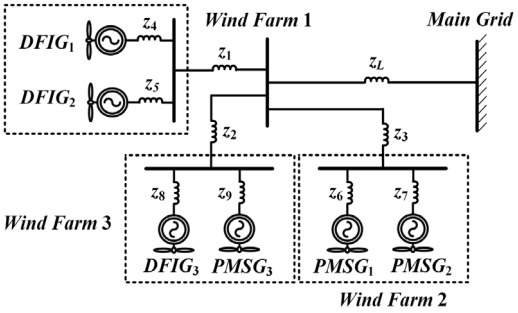

Fig. 7. Structure of the 1st example WPCS with 3 PMSGs and 3 DFIGs.

where C represents the capacitance, V_{dc} represents the DC voltage across the capacitor, P_r and P_g is the active power delivered by the rotor side converter (RSC) and GSC.

From Fig. 5 and Eq. (27), it can have:

$$\Delta I_{kd}^{ref} = \frac{K_{kvp}s + K_{kvi}}{C_{kdc}V_{kdc0}s^2}(\Delta P_{kr} - \Delta P_{kg}) = Q_k(s)\Delta P_k \tag{28}$$

Denoting $G_k(s)$ as the part of the kth PMSG excluding the dynamics described by the DC voltage control outer loops in Eq. (28). Consider the case that dynamics of L_1 DC voltage control outer loops of L_1 PMSGs and L_2 PLLs of L_2 DFIGs in the WPCS are similar ($L_1 + L_2 = L$) when their bandwidth is similar. Fig. 6 illustrates the division of the WPCS similar to Fig. 4, where the DC voltage control outer loops of L_1 PMSGs and the PLLs of L_2 DFIGs are subsystem $\boldsymbol{P}(s)$ and the rest of the WPCS is subsystem $\boldsymbol{W}(s)$.

Based on Fig. 6, analysis similar to that presented in the above subsection can be carried out to indicate that it is possible that the DC

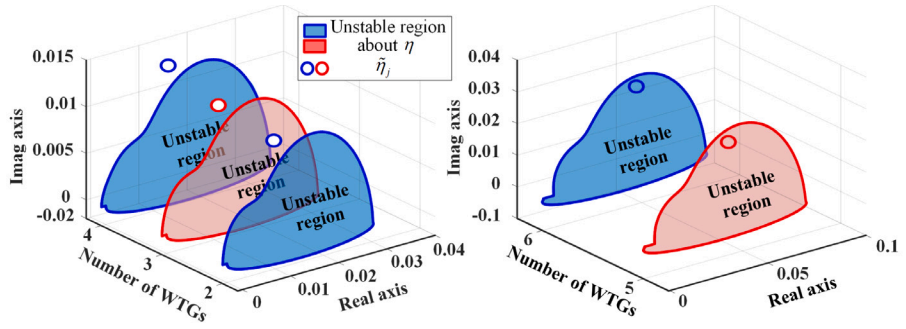

Fig. 8. Unstable regions about $\tilde{\eta}$ of the 1st example WPCS when the number of WTGs being connected, N, increased.

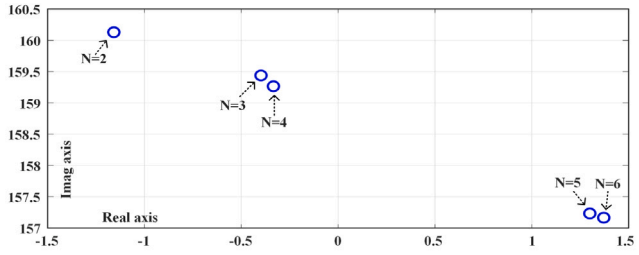

Fig. 9. Positions of dominant oscillation modes of the 1st example WPCS as N increased.

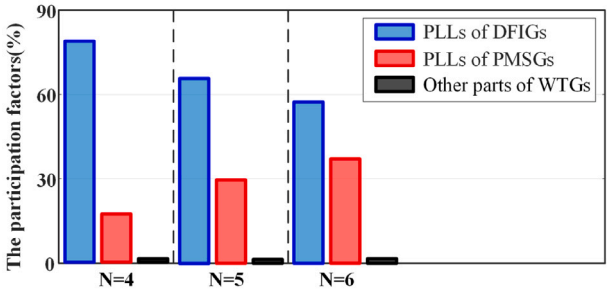

Fig. 10. Computational results of participation factors as the number of grid-connected WTGs varied — study case 1.

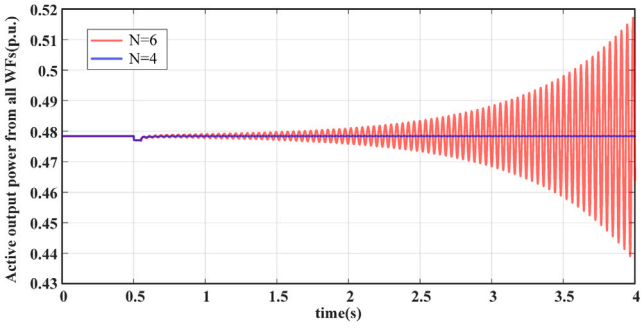

Fig. 11. Nonlinear simulation — study case 1.

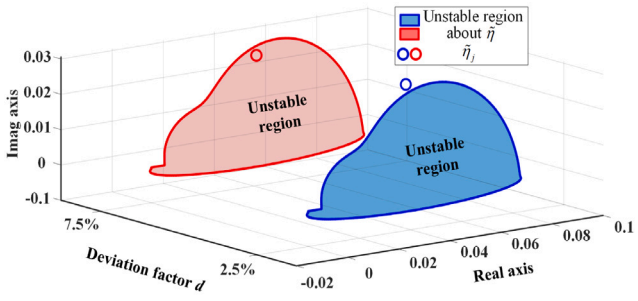

Fig. 12. Unstable region about $\tilde{\eta}$ of the 1st example WPCS when integral gain values of the PLLs were varied with N = 6.

voltage control outer loops of L_1 PMSGs and the PLLs of L_2 DFIGs may collectively introduce the risk of oscillatory instability of the WPCS.

3. Study cases — collective impact of the PMSGs and the DFIGs

3.1. Study case 1 — the 1st example WPCS

Structure of a WPCS comprised of 3 PMSGs and 3 DFIGs is depicted in Fig. 7. Dynamics of 3 PMSGs and 3 DFIGs are different. However, parameters of their PLLs are same and hence their PLLs are of the similar dynamics. The key parameters of the PMSGs and the DFIGs as well as the network are given in Table A.1. of Appendix.

Tests were conducted to evaluate and demonstrate the analysis made in the previous section about the risk of oscillatory instability brought about collectively by both the PMSGs and the DFIGs in the example WPCS. In the tests, only $DFIG_1$ and $DFIG_2$ were initially connected in the example WPCS. Afterwards, $PMSG_1$, $PMSG_2$, $DFIG_3$ and $PMSG_3$ were connected one by one (i.e., number of grid-connected WTGs, N, increased from N = 2 to N = 6). When one more WTG was connected, both the load flow condition of the example WPCS and the dynamics interactions between the WTGs changed. Those two factors (load flow condition and dynamic interactions) affected the oscillatory stability of the example WPCS. Since the analysis in the previous section is about the risk of oscillatory instability introduced by the dynamic interactions between the WTGs, in the tests the impact on the oscillatory stability of the change of load flow condition should be removed in order to achieve correct and reasonable evaluation and demonstration. Therefore, a particular design for the tests was implemented in the tests as follows.

Initially, the example WPCS were connected with $DFIG_1$ and $DFIG_2$ in addition to 4 constant power sources. Those 4 constant power sources were connected at the locations where $PMSG_1$, $PMSG_2$, $DFIG_3$ and $PMSG_3$ were connected respectively. The values of power output from a constant power source were as same as those of the WTG connected at the same location. Afterwards, the constant power sources were replaced one by one by $PMSG_1$, $PMSG_2$, $DFIG_3$ and $PMSG_3$ separately. Hence, when $PMSG_1$, $PMSG_2$, $DFIG_3$ and $PMSG_3$ were connected in the example WPCS, the load flow condition of the WPCS was unchanged and only the dynamics interactions among the WTGs varied. Subsequently, the tests ensure that any risk of oscillatory when N increased is caused only by the variation of dynamic interactions among

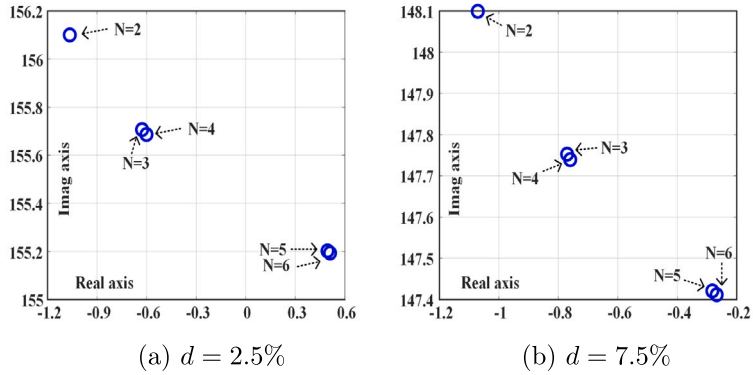

Fig. 13. Positions of dominant oscillation modes of the 1st example WPCS when integral gain values of the PLLs were varied and N increased.

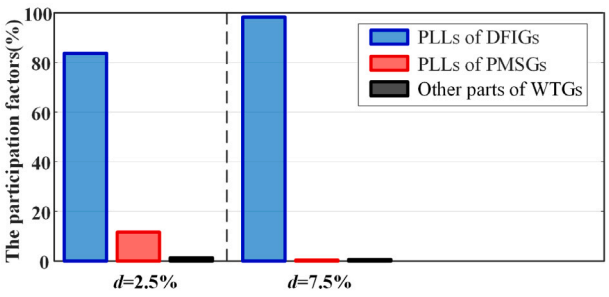

Fig. 14. Computational results of participation factors when integral gain values of the PLLs were varied — study case 1.

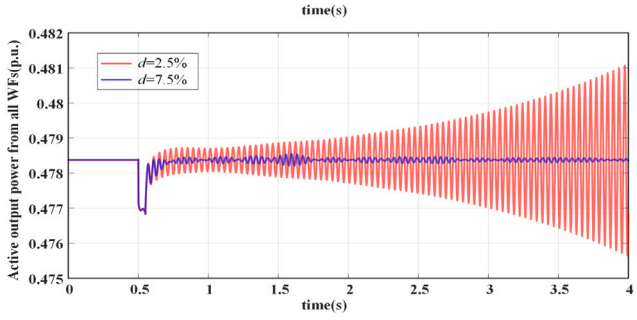

Fig. 15. Nonlinear simulation when integral gain values of the PLLs were varied — study case 1.

the WTGs. In the paper, this particular design for the tests that the WTG replace constant power source has been implemented in all the tests presented latter.

Based on Eq. (26), following function can be established:

$$\tilde{\lambda} = \frac{1}{2}[V_{n0}K_{np}(\tilde{\eta}-1) \pm j\sqrt{V_{n0}^2K_{np}^2(\tilde{\eta}-1)^2 + 4V_{n0}k_{ni}(\tilde{\eta}-1)}] \quad (29)$$

Eq. (29) defines the correspondence between the dynamic interaction $\tilde{\eta}$ between components with similar dynamic characteristics (in Study Case 1, the PLL) and the remaining part of the WPCS, as well as the oscillation mode a of the WPCS. For the 1st example WPCS, when different number (N) of the WTGs, were connected, the unstable region about $\tilde{\eta}$ was varied. Those unstable regions were calculated and are displayed in Fig. 8. In addition, when more WTGs (N increased) were connected (i.e., replacing the constant power sources), value of $\tilde{\eta}$, denoted as $\tilde{\eta}_j$, associated with the dominant oscillation mode of the 1st example WPCS ($\tilde{\lambda}$ with poorest damping) varied. Positions of $\tilde{\eta}_j$ when N increased are also displayed in Fig. 8.

Fig. 8 shows that when more WTGs were connected, the unstable regions about expanded. (For clarity, the results are shown in two separate subplots, and note that the scales of the two diagrams are different.) Subsequently, fell within the unstable regions when N was greater than 4. This is when the dominant oscillation mode was in the right-half of complex plane and the collective impact of the PMSGs and the DFIGs led to the oscillatory instability of the 1st example WPCS.

Fig. 9 illustrates the positions of the dominant oscillation modes after the WTGs were sequentially connected to the system. It can be seen that as more WTGs were connected, the dominant oscillation mode of the PLLs gradually shifted towards the right-hand side of the complex plane. When $DFIG_3$ was connected to the system, the dominant mode moved into right-half plane of the complex plane, indicating system instability. Furthermore, when $PMSG_3$ was connected, the dominant mode of the PLLs moved further to the right. Hence, Fig. 9 confirms the results presented in Fig. 8.

Fig. 10 shows the participation factors for the dominant oscillation modes, confirming that the dominant oscillation modes were related to the PLLs of both the PMSGs and the DFIGs such that it was the collective impact of the PLLs of the DFIGs and PMSGs causing the oscillatory instability of the 1st example WPCS.

Fig. 11 presents the nonlinear simulation results. At 0.5s, the system experienced a disturbance, causing a 5% decrease in the output power of $PMSG_1$, which lasted for 0.05 s. The non-linear simulation model is built in MATLAB/Simulink and includes the wind turbine units, the transmission network, and the external power system. The external power system is represented by a 4th-order synchronous generator, and the PMSGs and the DFIGs within the system are modeled using 15th-order models. Detailed modeling methods can be found in [26,31]. The oscillation frequency observed in Fig. 11 (about 25 Hz) matches that of the dominant oscillation mode identified in Fig. 9, calculated from its imaginary part as Imag/2π. This consistency between the nonlinear simulation and the eigenvalue analysis confirms that the oscillation is governed by the identified dominant mode.

In practice, parameters of PLLs may not be identical. To evaluate the collective impact of the PMSGs and the DFIGs when parameters of their PLLs are not the same, following tests were conducted.

The integral gain of the PLL for $PMSG_1$ served as the base value. The integral gain of the PLLs of other WTGs varied consecutively from that of $PMSG_1$ by a deviation factor d. Fig. 12 illustrates the unstable region about $\tilde{\eta}$ and the position of $\tilde{\eta}_j$ when all WTGs were connected (i.e., N = 6) and d respectively was 2.5% and 7.5%. From Fig. 12, it can be seen that when d was 2.5%, $\tilde{\eta}_j$ falls within the unstable region about $\tilde{\eta}$. Hence, even though the parameters of the PLLs were slightly varied, the collective impact of the PLLs of the DFIGs and PMSGs still caused the oscillatory instability of the 1st example WPCS. However, when d was 7.5%, $\tilde{\eta}_j$ was outside the unstable region about $\tilde{\eta}$ such that the collective impact did not lead to system instability. This test indicates that to increase the difference of values of the parameters of the PLLs

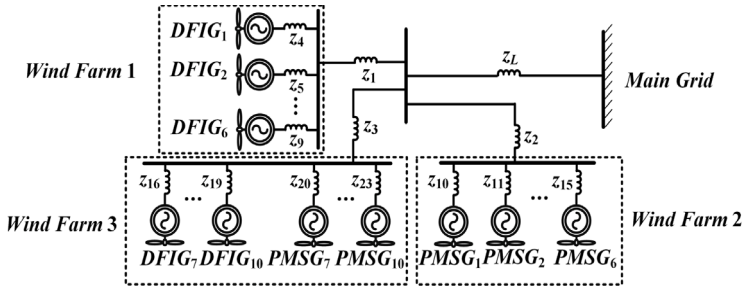

Fig. 16. Structure of the 2nd example WPCS with 10 PMSGs and 10 DFIGs.

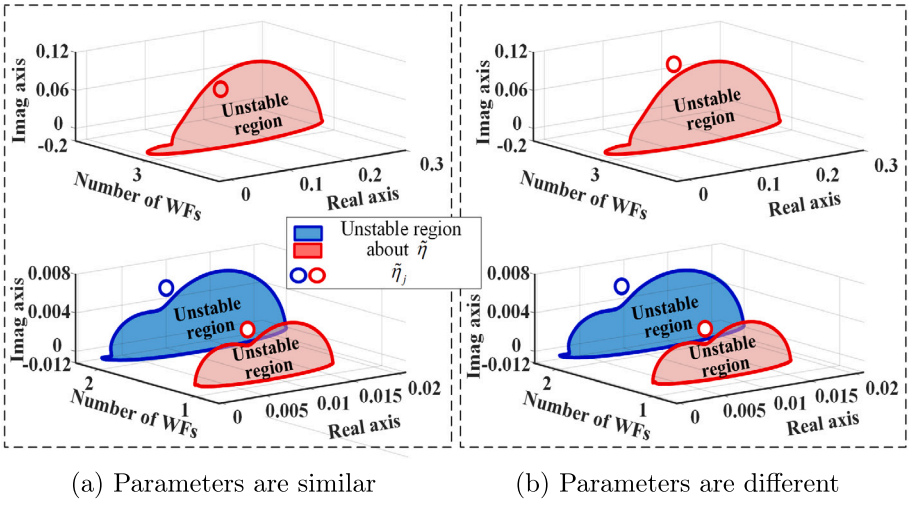

Fig. 17. Unstable region about $\tilde{\eta}$ of the 2nd example WPCS when the number of WFs being connected, M, increased.

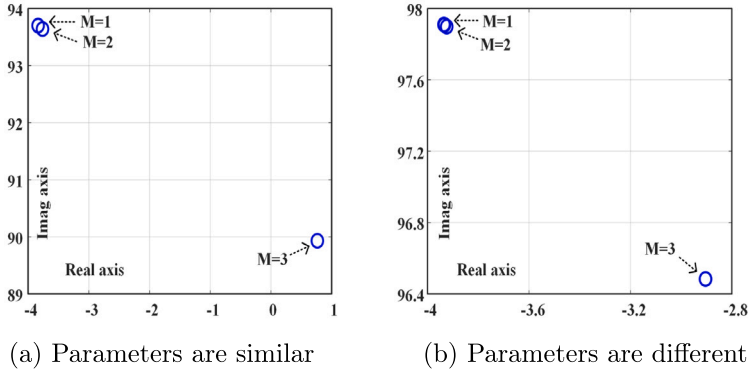

Fig. 18. Positions of dominant oscillation modes of the 2nd example WPCS for different x_L when the number of WFs being connected, M, increased.

can reduce the instability risk brought about by the collective impact. It means that the harmful collective impact was indeed from the similar dynamics of the PLLs equipped by the DFIGs and PMSGs.

Fig. 13 presents the positions of dominant oscillation modes when integral gain values of the PLLs were varied. In Fig. 13(a), the deviation factor d is 2.5%; in Fig. 13(b), the deviation factor d is 7.5%. Fig. 14 shows the participation factors of the dominant oscillation modes. Fig. 15 is the non-linear simulation. They confirm the results presented in Fig. 12.

Following observations can be made from the above test results of the 1st example WPCS:

(1) When more WTGs, either PMSGs or DFIGs, were connected, the risk of oscillatory instability increased.

(2) The instability risk was associated with all the WTGs, i.e., the PMSGs and the DFIGs.

(3) The harmful collective impact was indeed due to the similar dynamics of the PLLs equipped by the DFIGs and PMSGs.

3.2. Study case 2 — the 2nd example WPCS

The 2nd example WPCS, illustrated by Fig. 16, consists of 3 wind farms (WFs). 20 WTGs are classified into 8 groups as they are from 8 different manufacturers. Parameters of the WTGs are significantly different from a group to another. Following two cases are presented in this subsection: (a) Parameters of the PLLs equipped by 20 WTGs are similar, assuming that the manufacturers intend to achieve the similar phase tracking performance of the PLLs. (b) Parameters of the PLLs of the WTGs in 8 different groups are considerably different. The main parameters of 20 WTGs are given in Table A.2. of Appendix. Tests were carried out to evaluate the collective impact of the WTGs by connecting

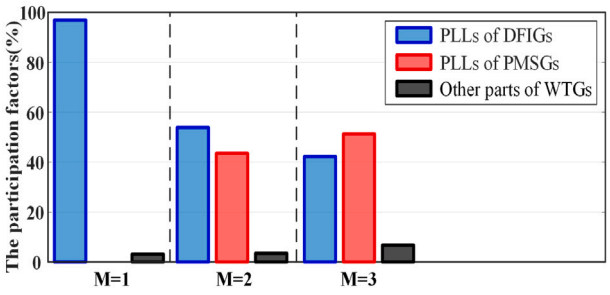

Fig. 19. Computational results of participation factors when the number of WFs being connected, M, increased — study case 2.

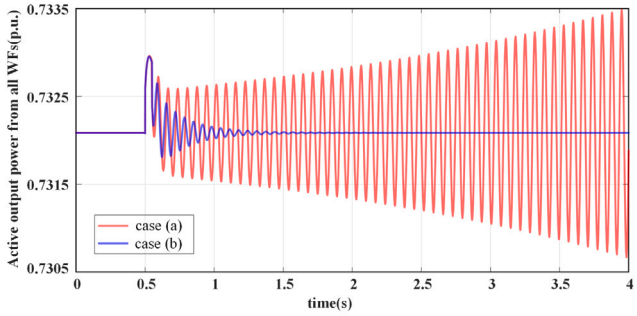

Fig. 20. Nonlinear simulation case (a) and case (b) — study case 2.

the WFs to the system in the following sequence: WF_1, WF_2, WF_3. The way to connect the WFs was similar to that described in the tests of study case 1 for the 1st example WPCS, i.e., by replacing the constant power sources with the WTGs.

Fig. 17 presents the computational results of the unstable regions about $\tilde{\eta}$ and the positions of $\tilde{\eta}_j$, when number of the WFs, M, connected to the system varied. It can be seen that when the WTGs in WF_3 were connected, $\tilde{\eta}_j$ fell within the unstable regions about $\tilde{\eta}$ in case (a), indicating the collective impact of the PLLs with the similar dynamics of the PMSGs and the DFIGs causing system instability. However, in case (b) when the dynamics of the PLLs in 8 different groups were considerably different, $\tilde{\eta}_j$ was outside the unstable regions about $\tilde{\eta}$, indicating that the system maintained being stable though 3 WFs were all connected. Note that when M was 3, the unstable regions about $\tilde{\eta}$ were expanded considerably as the scales of real and imaginary axis were 10 times of those when M = 1 and M = 2.

Fig. 18 shows the positions of dominant oscillation modes of the 2nd example WPCS on the complex plane as the number of WFs connected, M, changes. Fig. 19 presents the participation factor results for the dominant oscillation mode in case (a) when M varied. Fig. 20 gives the results of non-linear simulation with M = 3. At 0.5 s, the system was disturbed, causing a 5% increase in the output power of $PMSG_1$, which lasted for 0.05 s before returning to normal. They confirm the results shown in Fig. 17 that even parameters of the same type of WTGs, either PMSGs or DFIGs, are different, they can still induce growing oscillations if their PLLs are of the similar dynamics (case (a)). However, if the number of the PLLs with similar dynamics decreases, the risk of oscillatory instability decreases (case (b)).

In order to assess the impact of grid strength on the risk of oscillatory instability introduced by the collective impact, the following tests were conducted. When the parameters of PLLs are different, the transmission line reactance x_L (where the transmission line impedance $z_L = r_L + x_L$) is further increased to 0.2 p.u. and 0.3 p.u., resulting in a further reduction in grid strength.

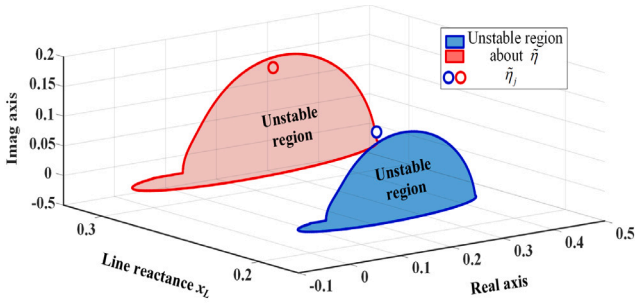

Fig. 21. Unstable region about $\tilde{\eta}$ of the 2nd example WPCS for different x_L when the number of WFs being connected, M, increased.

Fig. 21 illustrates the unstable region about $\tilde{\eta}$ and the positions of $\tilde{\eta}_j$ under different x_L values, when number of the WFs, M, connected to the system varied. It can be observed that although the differences in PLL parameters reduce the collective impact, when x_L increases to 0.3 p.u. after connecting WF_3, $\tilde{\eta}_j$ still falls within the unstable region. Meanwhile, the increase in x_L also significantly enlarges the unstable region of $\tilde{\eta}$.

Fig. 22 shows the positions of the dominant oscillation modes under different x_L when the number of WFs being connected. In Fig. 22(a), x_L = 0.2 p.u.; in Fig. 22(b), x_L = 0.3 p.u.. Fig. 23 presents the participation factor results for the dominant oscillation modes. Fig. 24 displays the outcomes of a non-linear simulation conducted with M = 3. They confirm the results in Fig. 21, showing that an increase in transmission line reactance, which corresponds to a decrease in grid strength, can increase the risk of oscillatory instability, even though the PLL dynamics of the PMSGs and the DFIGs exhibit significant differences.

3.3. Study case 3 — the 3rd example WPCS

In the previous study cases, test results are about the collective impact of the PMSGs and the DFIGs when their PLLs are of similar dynamics. This subsection presents test results on the collective impact of the WTGs, when the DC voltage control bandwidth of the PMSGs are similar to the bandwidth of the PLLs in the DFIGs, such that the DC voltage control in the PMSGs and the PLLs in the DFIGs are of the similar dynamics. Theoretical analysis for this case has been presented in Section 2.4 of previous section.

Fig. 25 shows the configuration of the 3rd example WPCS, consisting of 10 PMSGs and 10 DFIGs. Parameters of 10 PMSGs are same and those of 10 DFIGs are also same. It happens that the bandwidth of the DC voltage control loops of the PMSGs is as same as that of the PLLs of the DFIGs. Hence, though dynamics of the PMSGs are significantly different with those of the DFIGs, the DC voltage control of the PMSGs is of the similar dynamics with the PLLs of the DFIGs. The key parameters for the 3rd example of the WPCS are listed in Table A.3. of Appendix.

The arrangement to evaluate the collective impact of the PMSGs and the DFIGs is as same as that in the previous study cases, i.e., the PMSGs and the DFIGs were connected to the 3rd WPCS one by one by replacing constant power sources. The sequence of connecting the WTGs is connection of a PMSG after a DFIG and so on. Initially, $DFIG_1$ and $PMSG_1$ were connected. Then $DFIG_2$ was connected followed by the connection of $PMSG_2$ until 10 DFIGs and 10 PMSGs were all connected.

Fig. 26 shows the unstable region about $\tilde{\eta}$ when the number of WTGs, N, increased from 8 to 20. (For clarity, the results are shown in two separate subplots.) The positions of $\tilde{\eta}_j$ are also indicated in Fig. 26. It can be seen that when N is greater than 16, the corresponding $\tilde{\eta}_j$ falls into the unstable region about $\tilde{\eta}$. Subsequently, the collective

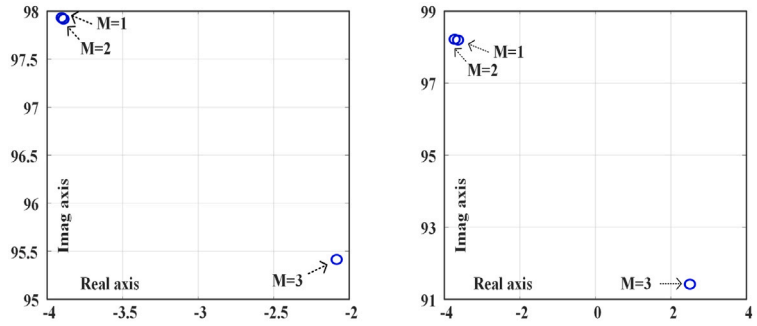

Fig. 22. Positions of dominant oscillation modes of the 2nd example WPCS for different x_L when the number of WFs being connected, M, increased.

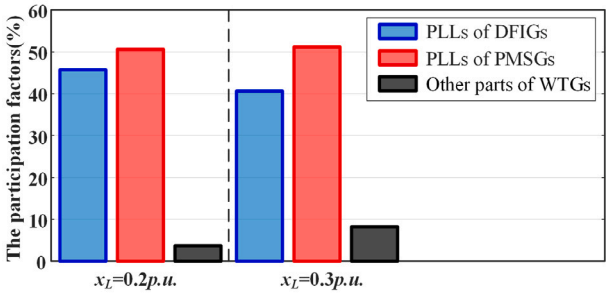

Fig. 23. Computational results of participation factors for different x_L values with M = 3 — study case 2.

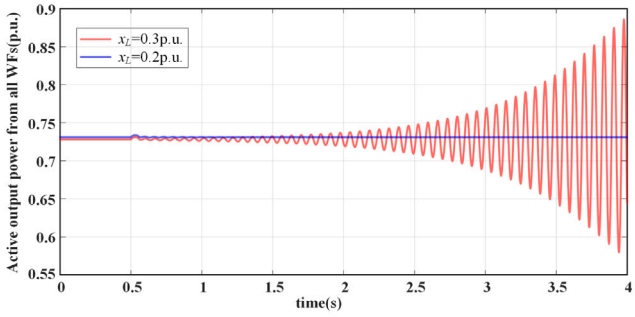

Fig. 24. Nonlinear simulation under different x_L with M = 3 — study case 2.

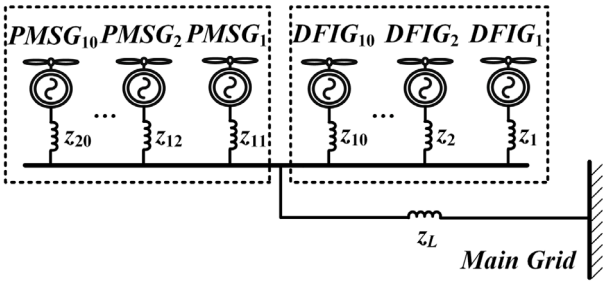

Fig. 25. Configuration of the 3rd example WPCS comprised of 10 PMSGs and 10 DFIGs.

impact of the PMSGs and the DFIGs led to the oscillatory instability of the 3rd example WPCS.

Fig. 27 gives the computational results of dominant oscillation mode when N increased. It validates that the collective impact of the PMSGs and the DFIGs caused the oscillatory instability when the number of the WTGs increased. Fig. 28 presents of computational outcomes for the participation factors of the dominant oscillation modes when N varied. It can be seen that the dominant oscillation modes are intimately associated with the DC voltage control loops of the PMSGs and the PLLs of the DFIGs. Hence, it confirms that the similar dynamics of the DC voltage control of the PMSGs and the PLLs of the DFIGs are the root cause of the collective impact of the PMSGs and the DFIGs.

The results of the non-linear simulation, presented in Fig. 29, provide confirmation. At 0.5 s, the system was disturbed, causing a 5% decrease in the output power of $DFIG_3$, which lasted for 0.05 s before returning to normal.

To evaluate the collective impact when the bandwidths of the DC voltage control of the PMSGs and the PLLs of the DFIGs differ, the following tests were conducted.

The integral gain of DC voltage control loop of $PMSG_1$ and that of the PLL of $DFIG_1$ were used as the base value. The integral gain of DC voltage control loops of other PMSGs was increased by a deviation factor, d, consecutively. The integral gain of the PLLs of other DFIGs was decreased consecutively by d. d was set to be 5% and 25%, respectively. Subsequently, bandwidths of the DC voltage control and the PLLs were varied in the tests.

Fig. 30 shows the unstable region about $\tilde{\eta}$ and the positions of $\tilde{\eta}_j$ when N was 20. It can be observed that when the bandwidth difference was small (d = 5%), the $\tilde{\eta}_j$ was still in the unstable region. The collective impact of the PMSGs and the DFIGs caused oscillatory instability of the 3rd example WPCS. However, when bandwidth difference was large (d = 25%), $\tilde{\eta}_j$ was outside the unstable region. The harmful collective impact of the PMSGs and the DFIGs was avoided.

Fig. 31 shows the positions of the dominant oscillation modes when N increased and bandwidths varied. In Fig. 31(a), the deviation factor d is 5%; in Fig. 31(b), the deviation factor d is 25%. Fig. 32 presents the participation factor results for the dominant oscillation modes. They confirm that similar dynamics for the DC voltage control loops of the PMSGs, as well as for the PLLs of the DFIGs, as measured by their bandwidths, are the root cause of harmful collective impact of the WTGs. The non-linear simulation results confirm this, as given in Fig. 33.

4. Conclusions

Previous studies have revealed that in a grid-connected wind farm, the same type of WTGs, either PMSGs or DFIGs, with similar dynamics may collectively bring about the risk of sustained oscillations. This collective impact exhibits as increasing risk of oscillations when more WTGs with similar dynamics are connected.

A wind power collecting system (WPCS) is comprised of multiple wind farms with the PMSGs and the DFIGs, dynamics of which are totally different. This paper investigates the oscillation instability collectively caused by both the PMSGs and the DFIGs, in the WPCS. By

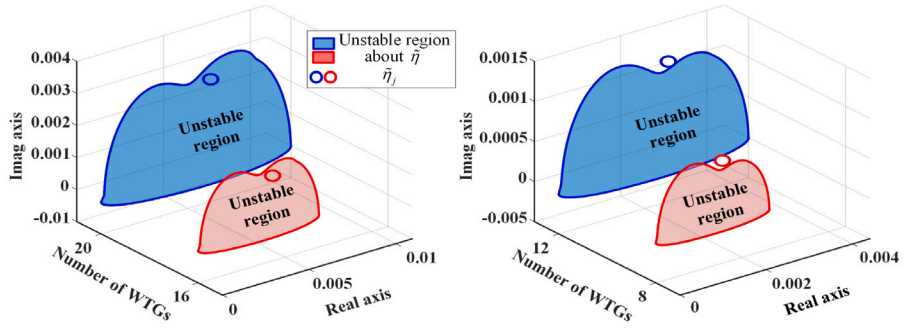

Fig. 26. Unstable regions about $\tilde{\eta}$ of the 3rd example WPCS when the number of WTGs being connected, N, increased — Study case 3.

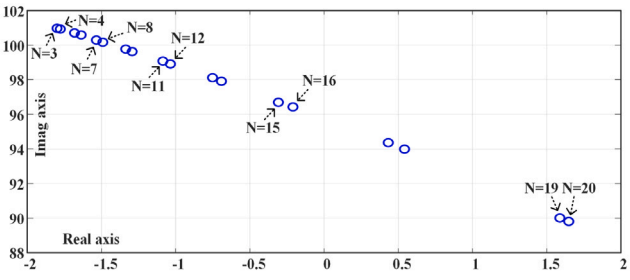

Fig. 27. Positions of dominant oscillation modes of the 3rd example WPCS as N increased.

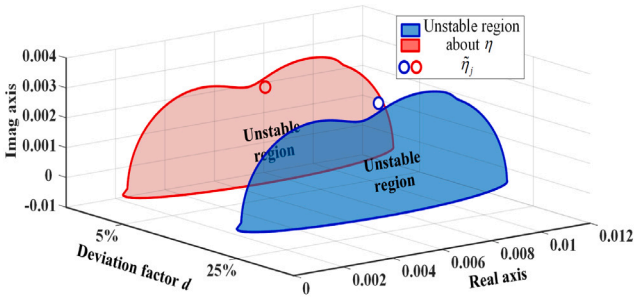

Fig. 30. Unstable regions about $\tilde{\eta}$ when the bandwidths differed by d.

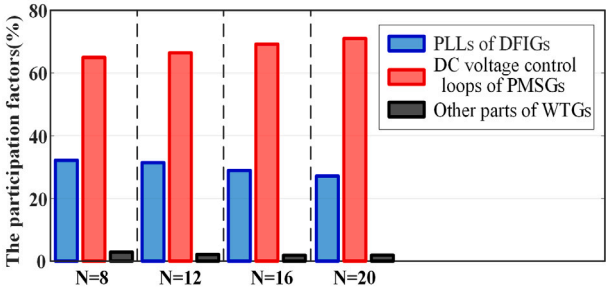

Fig. 28. Computational results of participation factors when N increased — study case 3.

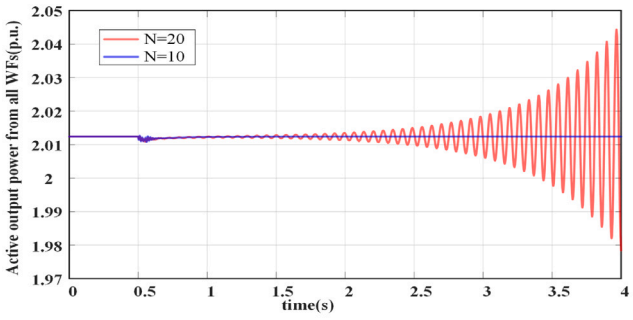

Fig. 29. Nonlinear simulation as N increased — study case 3.

using the PLLs as a representative type of components, the investigation analyzes why the PMSGs and the DFIGs, which are of the components with similar dynamics, may collectively cause the oscillatory instability of the WPCS. The analysis in the paper is extended to another representative case that the dynamics of the DC voltage control of the PMSGs are similar to the dynamics of the PLLs of the DFIGs. In this representative case, the PMSGs and the DFIGs may also collectively cause the oscillatory instability of the WPCS.

From the procedure of theoretical analysis presented in the paper, it is clear that the analysis can be extended to the following general case: if the dynamics of some components of the PMSGs are similar with the dynamics of some components of the DFIGs, the PMSGs and the DFIGs may collectively cause oscillatory instability of the WPCS. Hence, the study in the paper has made considerable advance from the previous studies about the collective impact in the following two aspects: (1) The collective impact of different types of the WTGs, both the PMSGs and the DFIGs, may also be dangerous; (2) The root cause of this dangerous collective impact is the components with similar dynamics, that are the parts of the PMSGs and the DFIGs.

Three case studies are provided to illustrate and assess the analysis and conclusions drawn in the paper. They clearly indicate that: (1) When the dynamics of the PLLs equipped by the PMSGs and the DFIGs are similar, the PMSGs and the DFIGs can collectively cause the growing oscillations; (2) If the dynamics of the DC voltage control in PMSGs resemble those of the PLLs in DFIGs, the PMSGs and the DFIGs can collectively cause the growing oscillations; (3) The risk of oscillations caused collectively by the PMSGs and the DFIGs increases when more PMSGs and DFIGs are connected in the WPCS; (4) When the similarity of dynamics of the components decreases, the risk of oscillations caused collectively by the PMSGs and the DFIGs decreases. (5) When the grid strength decreases, the risk of oscillations collectively caused by the PMSGs and the DFIGs increases.

Study presented in the paper is of practical significance to guide the operation and the planning of the WPCS as follows.

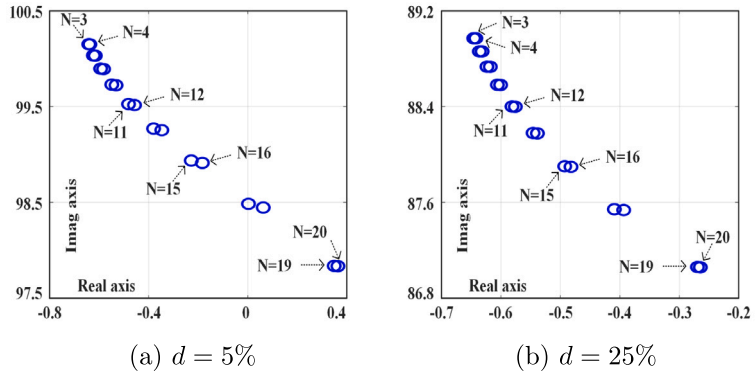

Fig. 31. Positions of dominant oscillation modes of the 3rd example WPCS under different d when N increased.

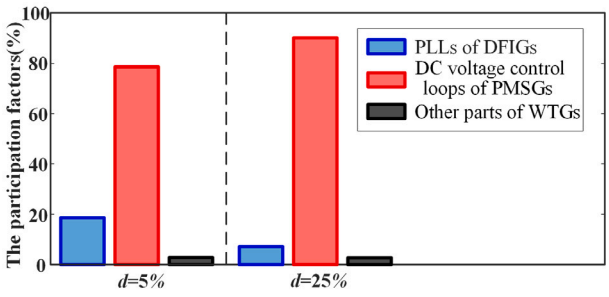

Fig. 32. Computational results of participation factors under different d with N = 20 — study case 3.

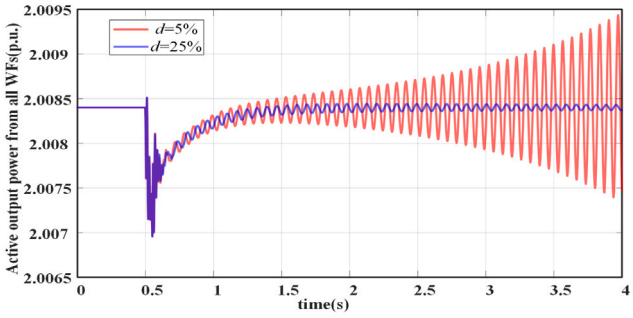

Fig. 33. Nonlinear simulation under different d with N = 20 — study case 3.

(1) In the operation of a practical WPCS, if it is found that growing oscillations occur when more WTGs are connected, it is possible that the oscillations may be caused by the collective impact of the WTGs. Further examination is needed to check whether the oscillations are closely related to the heavy loading of wind power. If they are not and there are components of the WTGs with similar dynamics, it can be certain that the components with similar dynamics are the root cause of growing oscillation. Tuning the parameters of those components to diversify their dynamics can reduce the risk of the oscillations.

(2) Dangerous collective impact may constrain the scale of a WPCS under planning. Normally, typical loading conditions, parameters and configurations of the WTGs are adopted in planning the WPCS. According to the analysis and conclusions made in the paper, the same types of the WTGs adopting the same loading conditions, parameters and configurations are the most dangerous scenario when the risk of oscillations caused by the collective impact is high. Planning advice should be given that the WPCS should consider to install the WTGs from different manufacturers, who should consider to diversify the setting of the converter control system parameters (including the PLLs) for the WTGs. This can reduce the risk of oscillations caused by the collective impact as being identified in planning the WPCS. In addition, a weaker grid can further aggravate the oscillation risk caused by the collective impact, and therefore the grid strength should also be taken into account in the planning stage.

CRediT authorship contribution statement

Zhengnan Zhao: Writing – review & editing, Visualization, Validation, Software, Formal analysis, Data curation. **Wenjuan Du:** Writing – original draft, Supervision, Resources, Project administration, Investigation, Funding acquisition. **Qiang Fu:** Supervision, Investigation. **Xiao Chen:** Methodology, Formal analysis, Data curation. **Yijun Wang:** Writing – original draft, Resources, Conceptualization. **H.F. Wang:** Writing – original draft, Supervision, Resources.

Declaration of competing interest

The authors declare that they have no known competing financial interests or personal relationships that could have appeared to influence the work reported in this paper.

Acknowledgments

This work was supported in part by the Engineering Special Team of Sichuan University on New Energy Power Systems, China and supported by the National Natural Science Foundation of China under Grant 52077144.

Appendix. Main parameters of the study case

See Tables A.1–A.3.

Data availability

Data will be made available on request.

Table A.1
The main parameters in 1st example WPCS (p.u.).

lines	$z_L = 0.001 + j0.2, z_{1-3} = 0.001 + j0.12, z_{4-9} = 0.0008 + j0.0128$
DFIGs	$K_{p\_PLL1-3} = 2.37, K_{i\_PLL1-3} = 82, C_{p1-3} = 13.29, P_{active1-3} = 0.08$
PMSGs	$K_{p\_PLL1-3} = 2.37, K_{i\_PLL1-3} = 82, C_{p1-3} = 30, P_{active1-3} = 0.08$

Table A.2
The main parameters in 2nd example WPCS (p.u.).

lines	$z_L = 0.0025 + j0.165, z_{1-3} = 0.0007 + j0.015, z_{4-6} = 0.0007 + j0.013,$ $z_{7-9} = 0.0007 + j0.0132, z_{10-12} = 0.0005 + j0.0105, z_{13-15} = 0.0005 + j0.0115,$ $z_{16,17} = 0.0009 + j0.018, z_{18,19} = 0.0005 + j0.0112, z_{20,21} = 0.0004 + j0.008,$ $z_{22,23} = 0.0006 + j0.0123.$
DFIGs	$P_{active1-3} = 0.028, P_{active4-6} = 0.035, P_{active7,8} = 0.022, P_{active9,10} = 0.04$ (a) $K_{p\_PLL1-10} = 8, K_{i\_PLL1-10} = 28.$ (b) $K_{p\_PLL1-10} = 7.90, 9.07, 8.45, 8.52, 8.57, 9.49, 9.32, 8.01, 7.83, 8.43.$ $K_{i\_PLL1-10} = 32.43, 28.35, 37.15, 36.08, 29.50, 32.52, 40.49, 34.58, 44.19, 31.52.$
PMSGs	(a) $K_{p\_PLL1-10} = 8, K_{i\_PLL1-10} = 28.$ (b) $K_{p\_PLL1-10} = 8.52, 9.04, 8.51, 8.42, 9.41, 8.72, 8.87, 9.37, 9.25, 8.63.$ $K_{i\_PLL1-10} = 30.01, 34.02, 41.38, 42.64, 26.64, 32.98, 36.20, 35.10, 38.94, 39.18.$

Table A.3
The main parameters in 3rd example WPCS (p.u.).

lines	$z_L = 0.001 + j0.0825,\ z_{1-20} = 0.001 + j0.015.$
DFIGs	$K_{p\_PLL1-10} = 4,\ K_{i\_PLL1-10} = 34,\ P_{active1-10} = 0.1.$
PMSGs	$C_{p1-10} = 17,\ P_{active1-10} = 0.1,\ K_{p\_GSC\_Udc1-10} = 0.15.,\ K_{i\_GSC\_Udc1-10} = 600.$

References

[1] Pryor SC, Barthelmie RJ. Wind shadows impact planning of large offshore wind farms. Appl Energy 2024;359. http://dx.doi.org/10.1016/j.apenergy.2024.122755.

[2] Cole M, Campos-Gaona D, Stock A, Nedd M. A critical review of current and future options for wind farm participation in ancillary service provision. Energies 2023;16(3). http://dx.doi.org/10.3390/en16031324.

[3] Andersson LE, Anaya-Lara O, Tande JO, Merz KO, Imsland L. Wind farm control - Part I: A review on control system concepts and structures. Iet Renew Power Gener 2021;15(10):2085–108. http://dx.doi.org/10.1049/rpg2.12160.

[4] Warder SC, Piggott MD. The future of offshore wind power production: Wake and climate impacts. Appl Energy 2025;380. http://dx.doi.org/10.1016/j.apenergy.2024.124956.

[5] Tan Y, Sun Y, Lin J, Yuan L, Su M. Revisit impedance-based stability analysis of VSC-HVDC system. IEEE Trans Power Syst 2024;39(1):1728–38. http://dx.doi.org/10.1109/tpwrs.2023.3234145.

[6] Negri S, Tironi E, Superti-Furga G, Carminati M. VSC-based LVDC distribution network with DERs: Equivalent circuits for leakage and ground fault currents evaluation. Renew Energy 2021;177:1133–46. http://dx.doi.org/10.1016/j.renene.2021.05.148.

[7] Hong L, Tang R, Jiang Q, Xie X, Zhu Y. Admittance-based stability analysis of LCL-type grid-connected inverter considering AC-side and AC-dc frequency coupling effects. IEEE Trans Power Deliv 2024;39(3):1351–63. http://dx.doi.org/10.1109/tpwrd.2024.3363031.

[8] Gupta AP, Mohapatra A, Singh SN. Measurement based parameters estimation of large scale wind farm dynamic equivalent model. Renew Energy 2021;168:1388–98. http://dx.doi.org/10.1016/j.renene.2020.12.063.

[9] Sun D, Liu H, Gong M, Chen Z, Hart P. A stability analysis tool for bulk power systems using black-box models of inverter-based resources. IEEE Trans Ind Appl 2023;59(6):7318–27. http://dx.doi.org/10.1109/tia.2023.3301488.

[10] Zhang Z, Qiao D, Wang Y, Xue J, Lin Y, Xue A. Analysis on subsynchronous/supersynchronous oscillations caused by limit intermittent saturation in positive damping PMSG integrated system. Electr Power Autom Equip 2023;43(9):33–8. http://dx.doi.org/10.16081/j.epae.202302003.

[11] Cai Z, Han J, Chen J, Gan D, Zhang H, Wang X. Analysis of D-Q small-signal impedance of back-to-back frequency converter. Front Energy Res 2023;11. http://dx.doi.org/10.3389/fenrg.2023.1288847.

[12] Zhu Y, Zhao J, Zeng Z, Mao L, Qu K. Impedance remodeling control strategy of grid-connected inverter with inertia-damping phase-locked loop under extremely weak grid. Int J Electr Power Energy Syst 2024;158:109961. http://dx.doi.org/10.1016/j.ijepes.2024.109961.

[13] Xiong L, Liu X, Liu Y, Zhuo F. Modeling and stability issues of voltage-source converter-dominated power systems: A review. Csee J Power Energy Syst 2022;8(6):1530–49. http://dx.doi.org/10.17775/cseejpes.2020.03590.

[14] Zhang C, Molinas M, Rygg A, Cai X. Impedance-based analysis of interconnected power electronics systems: Impedance network modeling and comparative studies of stability criteria. IEEE J Emerg Sel Top Power Electron 2020;8(3):2520–33. http://dx.doi.org/10.1109/jestpe.2019.2914560.

[15] Nian H, Liu Y, Li H, Hu B, Liao Y, Yang J. Commutation overlap characteristic modeling and stability analysis of LCC-HVDC in sending AC grid. IEEE Trans Sustain Energy 2022;13(3):1594–606. http://dx.doi.org/10.1109/tste.2022.3167106.

[16] Lyu J, Rao Y, Wang Z, Dai J, Cai X. Data-driven impedance identification and stability online assessment of wind farm connected with MMC-HVDC. IEEE Trans Ind Appl 2024;60(2):2567–76. http://dx.doi.org/10.1109/tia.2023.3333760.

[17] Liang C, Zuo X, Li J, Liu R, Huang C. Stability analysis of doubly-fed fan with small disturbance oscillation based on regional decoupling impedance model. Int J Electr Power Energy Syst 2024;162:110236. http://dx.doi.org/10.1016/j.ijepes.2024.110236.

[18] Tan X, Li C, Liu D, Wang H, Xu R, Lu X, et al. Multi-time scale model reduction strategy of variable-speed pumped storage unit grid-connected system for small-signal oscillation stability analysis. Renew Energy 2023;211:985–1009. http://dx.doi.org/10.1016/j.renene.2023.04.134.

[19] Yi Y, Zhou Y, Feng D, Yin W, Li H, Yang Q. Stability control and analysis of hydrogen production using a multi-terminal DC EV charging system with PV. Renew Energy 2024;234. http://dx.doi.org/10.1016/j.renene.2024.121196.

[20] Ide T, Hirase Y, Yoshimura E, Umezu Y, Bando S, Sugimoto K. Investigating and addressing synchronous instabilities in inverter-based resources within microgrids. Appl Energy 2025;377. http://dx.doi.org/10.1016/j.apenergy.2024.124379.

[21] Martinez JC, Amenedo JLR, Gomez SA, Alonso-Martinez J. Grid-forming control of doubly-fed induction generators based on the rotor flux orientation. Renew Energy 2023;207:162–76. http://dx.doi.org/10.1016/j.renene.2023.02.133.

[22] Tan X, Li C, Liu D, Wang H, Xu R, Lu X, et al. Multi-time scale model reduction strategy of variable-speed pumped storage unit grid-connected system for small-signal oscillation stability analysis. Renew Energy 2023;211:985–1009. http://dx.doi.org/10.1016/j.renene.2023.04.134.

[23] Li Q, Chen W, Wei Z, Kang Z, Tang Y. Stability and modal analysis of a DFIG-based wind energy conversion system under stator voltage vector control. Int J Electr Power Energy Syst 2024;162:110286. http://dx.doi.org/10.1016/j.ijepes.2024.110286.

[24] Du W, Wang Y, Wang HF, Yu J, Xiao X. Collective impact of multiple doubly fed induction generators with similar dynamics on the oscillation stability of a grid-connected wind farm. IEEE Trans Power Deliv 2021;36(5):2942–54. http://dx.doi.org/10.1109/tpwrd.2020.3030645.

[25] Du W, Wang Y, Wang Y, Wang HF, Xiao X. Analytical examination of oscillatory stability of a grid-connected PMSG wind farm based on the block diagram model. IEEE Trans Power Syst 2021;36(6):5670–83. http://dx.doi.org/10.1109/tpwrs.2021.3077121.

[26] Du W, Wang H. Analysis of power system sub/super-synchronous oscillations caused by grid-connected wind power generation. Springer Nature; 2023, http://dx.doi.org/10.1007/978-3-031-35343-7.

[27] Dong W, Du W, Xie X, Wang HF. An approximate aggregated impedance model of a grid-connected wind farm for the study of small-signal stability. IEEE Trans Power Syst 2022;37(5):3847–61. http://dx.doi.org/10.1109/tpwrs.2021.3138107.

[28] Yu J, Li J, Hu W, Zhang G, Wang H, Huang Q, et al. Small-signal modeling of wind farm with direct-drive PMSG using the component connection method. Energy Rep 2021;7:334–42. http://dx.doi.org/10.1016/j.egyr.2021.01.061.

[29] Huang B, Sun H, Liu Y, Wang L, Chen Y. Study on subsynchronous oscillation in D-PMSGs-based wind farm integrated to power system. Iet Renew Power Gener 2019;13(1):16–26. http://dx.doi.org/10.1049/iet-rpg.2018.5051.

[30] Liu Q, Zhang L, Qian Q. Fast LADRC-type phase-locked loop with adaptive extended state observer. IEEE Trans Ind Electron 2024;71(8):8268–78. http://dx.doi.org/10.1109/tie.2023.3317863.

[31] IEEE guide for synchronous generator modeling practices and parameter verification with applications in power system stability analyses. 2020, p. 1–92. http://dx.doi.org/10.1109/ieeestd.2020.9020274, IEEE Std 1110-2019 (Revision IEEE Std 1110-2002).